Redox Reactivity as the Controlling Element in Coordination Polymer Stereochemistry: Redox-Switched Growth Mechanism in the $[Fe^{II}-CN-Pt^{IV}]_n$ System

Clark Chang, David Ludwig, and Andrew Bocarsly*

Frick Laboratory, Princeton University, Princeton, New Jersey 08544

Received April 7, 1998

Coordination oligomers and polymers composed of $[(CN)_5Fe^{II}-CN-Pt^{IV}(NH_3)_4]$ units have been synthesized. The oligomer growth mechanism is based on the oxidation state of the iron centers which can be specified either chemically or electrochemically to allow control over oligomer structure. Cyclic voltammetry is found to be a sensitive probe of oligomer and polymer structure. ^{13}C NMR is also shown to be a useful technique for characterizing the different geometric isomers. Thin films composed of $[-(NC)_5Fe^{II}-CN-Pt^{IV}(NH_3)_4-]_n$ were electropolymerized onto transparent indium tin oxide (ITO) electrode surfaces and characterized with regard to polymer morphology.

Introduction

Mixed-valent inorganic complexes have received considerable interest because of their potential application to energy conversion, information storage, and photocatalysis. We previously reported the synthesis, characterization, and chemistry of the three-metal-center cyanide-bridged complex $\{[Pt(NH_3)_4]_2^{4+}\}\{[(NC)_5Fe^{II}-CN-Pt^{IV}(NH_3)_4-NC-Fe^{II}(CN)_5]^{4-}\}$[1] **(1)**. This complex has an Fe(II) → Pt(IV) intervalent charge-transfer absorption in the visible region of the spectrum ($\lambda_{max} = 425$ nm). We have focused our attention on **1** because irradiation into this band causes a one-photon, two-electron charge transfer. Work in our group has included analysis of the photochemical charge transfer in the trinuclear complex and analogues where the ligands on the Fe have been substituted,[2] the end metal centers have been replaced with Ru or Os,[2] and the central platinum has been ligand substituted.[3] We have also reported the modification of an ITO surface with $[-(NC)_5Fe^{II}-CN-Pt^{IV}(NH_3)_4-]_n$, formed by electropolymerization of **1**.[4] We are able to photochemically pattern the film into complex shapes and use it as a photochemical reagent for the spatial deposition of a variety of cyanometalate species.[5] One demonstrated application of this chemistry is the formation of an electrochemically switchable optical diffraction grating.[6]

We report here the synthesis and characterization of oligomers of the trinuclear complex, as well as an in-depth characterization of the polymer surface. Combining tetraammineplatinum(II) nitrate and potassium ferricyanide in aqueous solution cleanly yields the three-metal complex **1**. This product only contains iron in the Fe(II) oxidation state. There is no reaction between $Pt(NH_3)_4^{2+}$ and ferrocyanide; thus further formation of cyanide bridges to form higher order multinuclear complexes does not occur. Once compound **1** is available, reoxidation of the irons in this complex in the presence of additional tetraamminoplatinate can be employed to generate larger complexes with more metal centers.

We have dubbed these series of supramolecular complexes "hexacyanoferro platinum ammine", shortened to HCFPA. Complex **1** can then be written as $\{[Pt(NH_3)_4]_2^{4+}\}$[3-HCFPA]$^{4-}$, where the number in front of the abbreviation specifies the number of metal centers in the central molecule, in this case 2 irons and 1 platinum. The oligomer made by connecting two molecules of **1** through coordination to $Pt(NH_3)_4^{2+}$ is 7-HCFPA, a 7-metal oligomer composed of 4 irons and 3 platinums. As larger oligomers are formed, one can envision structures which are either one-dimensional (based on growth solely from terminal iron units) or are of higher dimensions if internal iron units are redox reactive and thus are reagents for the formation of bridging cyanide units. A complex mixture of branched chains will be referred to as poly-HCFPA.

We propose the synthetic strategy in Scheme 1 for longer chain oligomers of one dimension with counterions and ligands omitted for clarity.

Scheme 1

step 1: initiation

$$[\text{3-HCFPA}]^{4-} + \text{ox} \rightarrow [\text{3-HCFPA}]^{2-}$$

step 2: chain propagation

$$[\text{3-HCFPA}]^{2-} + Pt^{2+} + [\text{3-HCFPA}]^{2-} \rightarrow [\text{7-HCFPA}]^{2-}$$

$$[\text{7-HCFPA}]^{2-} + Pt^{2+} + [\text{7-HCFPA}]^{2-} \rightarrow [\text{15-HCFPA}]^{2-}$$

$$[\text{7-HCFPA}]^{2-} + Pt^{2+} + [\text{3-HCFPA}]^{2-} \rightarrow [\text{11-HCFPA}]^{2-}$$

...

$$[n\text{-HCFPA}]^{2-} + Pt^{2+} + [m\text{-HCFPA}]^{2-} \rightarrow [(n+m+1)\text{-HCFPA}]^{2-}$$

step 3: termination

$$[n\text{-HCFPA}]^{2-} + \text{red} \rightarrow [n\text{-HCFPA}]^{4-}$$

* To whom correspondence should be addressed.

(1) Zhou, M.; Pfennig, B. W.; Steiger, J.; Van Engen, D.; Bocarsly, A. B. *Inorg. Chem.* **1990**, *29*, 2457−2460.
(2) Pfennig, B. W.; Bocarsly, A. B. *J. Phys. Chem.* **1992**, *96*, 226−233.
(3) Wu, Y.; Cohran, C.; Bocarsly, A. B. *Inorg. Chim. Acta* **1994**, *226*, 251−258.
(4) Pfennig, B. W.; Bocarsly, A. B. *Inorg. Chem.* **1991**, *30*, 666−672.
(5) Bocarsly, A. B.; Chang, C. C.; Wu, Y.; Vicenzi, E. P. *J. Chem. Educ.* **1997**, *74*, 663−667.
(6) Wu, Y.; Pfennig, B. W.; Vicenzi, E. P.; Bocarsly, A. B. *Inorg. Chem.* **1995**, *34*, 4262−4267.

10.1021/ic980390e CCC: $15.00
Published on Web 10/02/1998

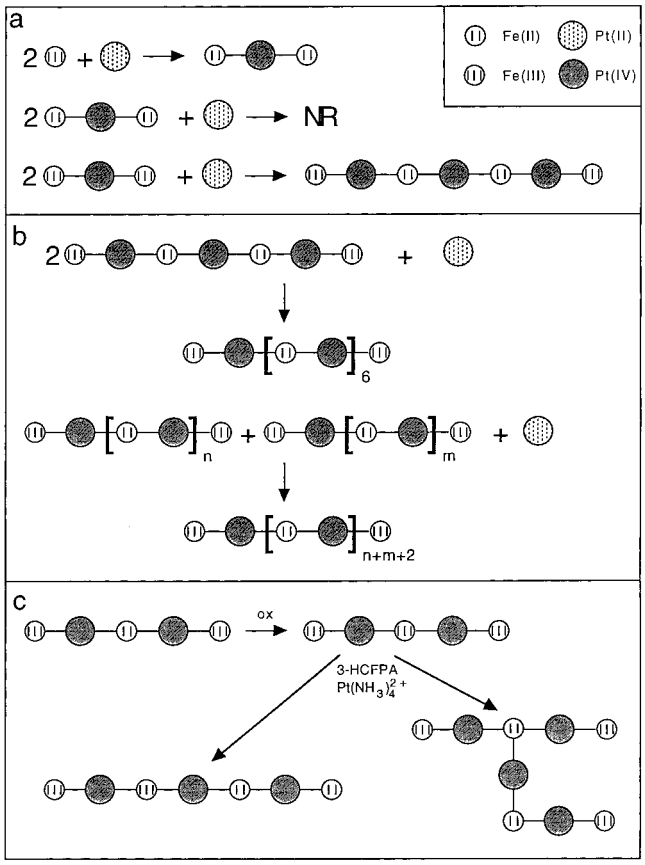

Figure 1. Redox-switched growth mechanism for oligomer species. (a) Only oxidized irons can be used to form linkages with Pt. Two oligomer units can combine together either as a straight chain (b) or as branches (c).

This mechanism closely resembles that of a step polymerization, where monomers react to form dimers, and these dimers can continue reacting to form trimers and tetramers until eventually large polymer molecules containing large numbers of monomer molecules are formed.[7] One feature of this proposed strategy is that the entire polymerization process takes place in one dimension; there is no branching. That is, polymer growth can only occur from the terminal iron positions. After two molecules of $[3\text{-HCFPA}]^{2-}$ react, all the interior irons in the resulting 7-metal oligomer are in the reduced state; only the terminal irons are left in the oxidized state and are capable of reacting further (Figure 1a). This is true for all the oligomers formed in this set of reactions, and thus, this synthetic strategy results in linear polymerization (Figure 1b). Chain extension continues as long as both reactants, oxidized iron centers and $Pt(NH_3)_4^{2+}$, are present. Thus, optimizing the yield of a particular chain length can be done either by adding a reducing agent, which reduces the terminal irons at a particular time after the reaction is started, thereby terminating chain growth, or by starting with a limiting amount of platinum complex. Central to this synthetic approach is the fact that oxidizing agent is only present in step 1; therefore, only 3-HCFPA is subject to oxidation. The coupling agent, $Pt(NH_3)_4^{2+}$, is added to the reaction mixture only after the oxidizing initiator has been consumed or removed; thus, reoxidation of internal irons is precluded, and only unreacted terminal irons are available to the chain reaction (step 2). Size exclusion chromatography can be employed to separate the mixture of oligomers.

(7) Odian, G. *Principles of Polymerization*, 3rd ed.; John Wiley & Sons: New York, 1991; p 768.

Oligomers of higher dimensionality can be synthesized via chain growth from the interior irons of the oligomer. Oxidation of the cyanoferrate units interior to the oligomer can be accomplished either by having oxidizing agent present in the reaction mixture after step 1 of Scheme 1 has been completed or by electrochemically oxidizing the internal iron units in the presence of $Pt(NH_3)_4^{2+}$. This variation in synthetic approach leads to branched structures as illustrated in Figure 1c. If the interior irons are continuously reoxidized after reaction, then the branches can be connected at various points along their lengths to form cross-links to produce a three-dimensional polymer. Thus by control of the reaction oxidation conditions, one can in principle produce oligomers or polymers having specific topographies based on the proportions of bridged cyanide ligands to iron centers. For clarity, irons with bridging cyanides will be represented in this text as $(\mu\text{-CN})_i\text{Fe}$ where the value of i indicates the number of bridging cyanides per iron center. Using this approach, synthetic strategies for the production of supramolecular systems having selective one-dimensional, two-dimensional (sheet structure), or three-dimensional (network structure) topologies can be developed.

Experimental Section

Chemicals. Tetraammineplatinum nitrate and Sephadex G-10, G-15, G-25, and G-50 gel filtration packings were from Aldrich, potassium nitrate, sodium nitrate, and potassium ferricyanide were from Fisher, and sodium dithionite was from J. T. Baker. All chemicals were reagent grade and were used without further purification. Deionized reverse osmosis purified water was used as the solvent in all cases.

Electrode Materials. Soda-lime glass sheets coated on one side with ITO to $\rho_s < 40\ \Omega$ (~300 nm thickness) were from Delta Technologies, Limited. H31 electrically conducting silver epoxy from Epoxy Technology was used to attach bare copper wire to the ITO-coated glass sheets.

Instruments. Cyclic voltammetry was performed using either a PINE RDE4 potentiostat or a PAR 273A potentiostat under computer control running PAR270 software. In either case, a large-area platinum foil counter electrode and a saturated calomel (SCE) reference electrode were employed. All potentials are reported versus SCE.

Nuclear magnetic resonance spectroscopy was performed using a JEOL GSX-500 NMR spectrometer. For ^{13}C NMR, the spectrometer was operated at a carbon frequency of 125.65 MHz. A 10 mm sample tube was employed which contained a 3 mm coaxial capillary tube holding tetramethylsilane (TMS = 0.0 ppm) in deuterated acetone for reference and lock, respectively. For ^{15}N NMR, the spectrometer was operated at 50.55 MHz. The same sample tube was used except with $Na^{15}NO_3$ in deuterium oxide in the reference tube. All spectra were referenced against $^{15}NO_3^- = 0$ ppm.

A Hewlett-Packard 8453 diode array spectrophotometer was used for UV−visible spectroscopy and interferometry. A Coherent 70-4 argon ion laser was used to generate 488 nm light. Profilometry was performed with a DEKTAK IIA from the Sloan Technology Corp.

Preparation of $Na_4[Fe(CN)_6-\{Pt(NH_3)_4\}-Fe(CN)_6]$ (3-HCFPA). Two hundred milligrams of $Pt(NH_3)_4(NO_3)_2$ and 400 mg of potassium ferricyanide were dissolved separately in 5 mL of deionized water. The two solutions were mixed, and the resultant solution was immediately passed through a sodium cation exchange column (40 mL of Amberlite IR-120 charged with 50 mL of NaCl solution) to remove any unreacted $Pt(NH_3)_4^{2+}$. The impure complex was collected and placed at the head of a Sephadex G-10 column (22 mm diameter, 100 cm length) and eluted with deionized water. The first red band was collected and allowed to dry under a stream of air at room temperature. All processes were carried out under low ambient light conditions because of the photoreactive nature of the product.

Synthesis and Chromatographic Separation of $Na_4[Fe(CN)_6-Pt(NH_3)_4-Fe(CN)_6-Pt(NH_3)_4-Fe(CN)_6-Pt(NH_3)_4-Fe(CN)_6]$ (7-HCFPA). 3-HCFPA was oxidized by adding ~150 mg of PbO_2 and ~0.5 mL of 1M H_2SO_4 to a 10 mL solution of 150 mg of

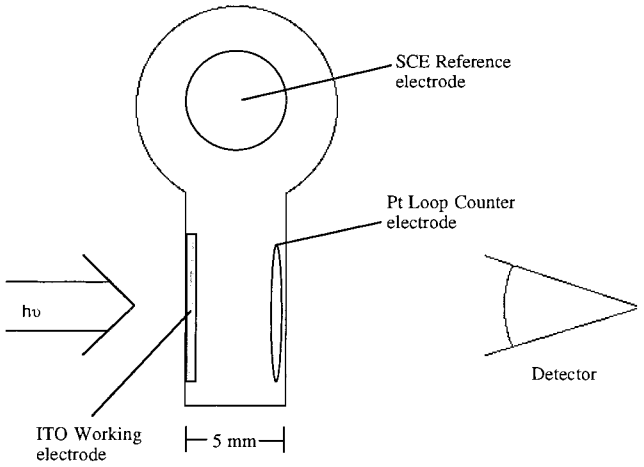

Figure 2. Experimental setup for in situ UV−vis characterization.

3-HCFPA. The solution was stirred for 5 min, after which the color changed from red to green. The solution was then filtered to remove the PbO_2, and 2.0 M NaOH was added dropwise until the pH of the solution was 7−8. Addition of a 0.5 M solution of $Pt(NH_3)_4^{2+}$ to this solution caused a color change to a dark red over a period of about 30 min. Product distribution could be optimized for a particular chain length by variation of the amount of added Pt; for example, 7-HCFPA is the dominant product when $[3\text{-HCFPA}]^{2-}$ and $Pt(NH_3)_4^{2+}$ are reacted in a 2:1 ratio.

The distribution of products formed from this oligomer synthesis was separated by size exclusion chromatography. Integration of the cyclic voltammogram waves recorded in the electrochemical analysis of the eluting product was used to characterize the fractions (see Results and Discussion for explanation of electrochemistry and notation). The ratio of doubly to singly bridged iron [(μ-CN)$_2$Fe/(μ-CN)$_1$Fe] was calculated and compared to the expected values for specific chain length. Because all the oligomers synthesized had a net charge of −2, it was expected and experimentally confirmed that the chromatographic columns separated oligomers only on the basis of the size of the product, with longer chain lengths eluting first and unreacted 3-HCFPA eluting last.

A loading of ∼1% of total column volume for a 1 m column of Sephadex G-50 was optimal for separating the longest chain lengths, and a 1 m column of Sephadex G-10 was sufficient for initial rough isolation of 7-HCFPA. This could be further refined with a 2.3 m column of G-25, where multiple yellow, orange, or red bands could be visually located and separated. 7-HCFPA, 11-HCFPA, and 15-HCFPA were separated cleanly in sufficient yields for NMR spectroscopy using this procedure, although oligomer lengths of up to 55-HCFPA were separated and identified. 7-HCFPA was chosen for further characterization.

Preparation of $[-(NC)_5Fe^{II}-CN-Pt^{IV}(NH_3)_4-]_n$ (Poly-HCFPA). Indium tin oxide coated soda-lime glass sheets were cut into 1.5 × 4 cm strips, and a copper wire was attached to one end with silver epoxy. A conventional three-electrode experimental setup was used with a SCE reference electrode. An ITO working electrode and Pt foil counter electrode were immersed plane parallel approximately 1 cm from each other in a solution of 5 mM $K_3Fe(CN)_6$, 5 mM $Pt(NH_3)_4(NO_3)_2$, and 0.1 M $NaNO_3$. A PAR 273A potentiostat was used to control time and potential of polymerization. After derivatizing, the ITO electrode was removed from solution, rinsed with deionized water, and allowed to dry before further analysis. In situ experiments were conducted in specially made glassware (Figure 2) with a solution containing 0.1 M $NaNO_3$ and 1 mM of each metal salt.

Results and Discussion

Synthesis and Morphology Control of Iron−Platinum Cyanometalate Oligomers. Cyclic voltammetry is a useful analytical tool for characterizing the oligomers since the $[Fe^{III/II}(CN)_6]^{3-/4-}$ redox potential is strongly dependent on the number of bridging −CN− ligands around a particular Fe center. The 3-metal complex **1** exhibits a single 2-electron cyclic voltammetric wave at $E_{1/2}$ = 0.54 V vs SCE[1] in contrast to the 1-electron wave at $E_{1/2}$ = 0.18 V vs SCE observed for free ferrocyanide in solution (Figure 3a). Electrochemical analysis of 7-HCFPA shows growth of an additional wave at 0.85 V vs SCE (Figure 3b), and poly-HCFPA exhibits waves at 0.54, 0.85, and 1.05 V vs SCE (Figure 3c). Formation of a CN−Pt bond inductively stabilizes the CN-π* orbital, thereby lowering the t_{2g} orbital energy associated with ferrocyanide. This results in a shift of the $[Fe^{III/II}(CN)_6]^{3-/4-}$ redox potential to more positive values with each additional bridging cyanide (Figure 4). Thus, the wave at $E_{1/2}$ = 0.54 V has been assigned to (μ-CN)$_1$Fe and the other waves have been assigned to (μ-CN)$_2$Fe and (μ-CN)$_3$Fe, respectively.

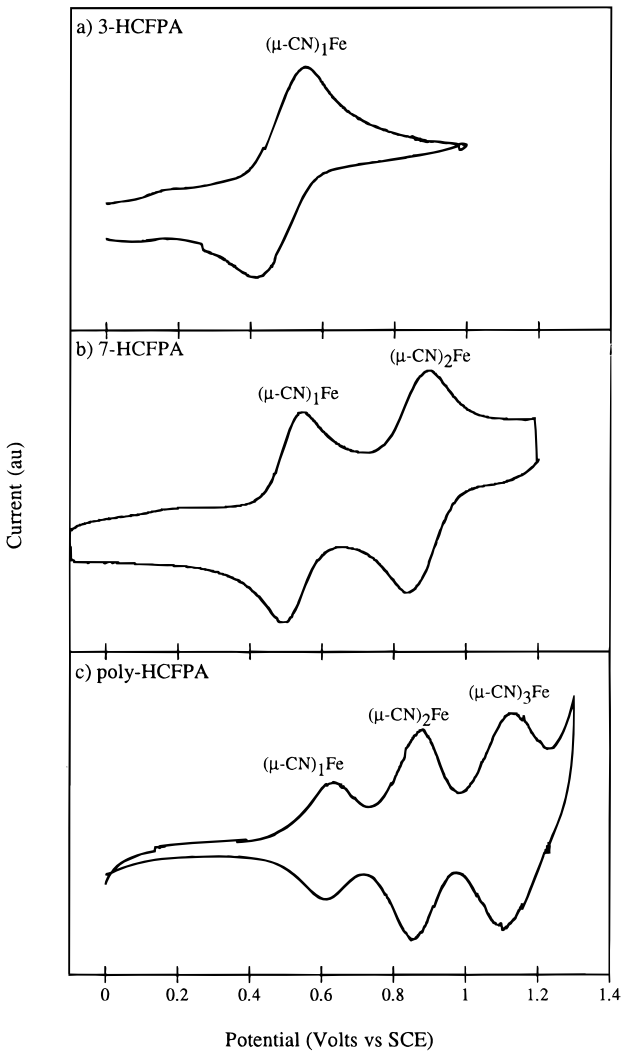

Figure 3. Cyclic voltammograms of (a) 3-HCFPA showing a single wave at 0.54 V, (b) 7-HCFPA with an additional wave at 0.85 V corresponding to doubly bridged iron, and (c) poly-HCFPA showing a wave at 1.1 V for triply bridged iron species. All experiments were run with 0.1 M $NaNO_3$ as supporting electrolyte.

The integrated area under the cyclic voltammetric waves can be used to characterize chain length. For example, a pure sample of 7-HCFPA is expected to exhibit two cyclic voltammetric waves, one corresponding to (μ-CN)$_1$Fe and the other to (μ-CN)$_2$Fe (Figure 3b). Since there are two of each type of iron in 7-HCFPA, the area under each of these waves should be equal; that is, the ratio of (μ-CN)$_2$Fe to (μ-CN)$_1$Fe is 1. A similar calculation for longer oligomers is summarized in Table

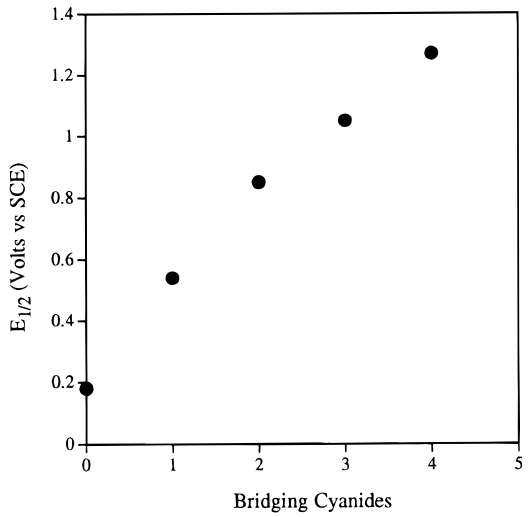

Figure 4. Increase of the iron redox potential within the polymer with the number of bridging cyanides around the iron center. Redox potentials presented here were obtained from ferricyanide in solution and from surface-modified-polymer cyclic voltammograms.

Table 1. Ratio of $(\mu\text{-CN})_2\text{Fe}$ to $(\mu\text{-CN})_1\text{Fe}$ for Various Oligomers

chain length	theoretical	experimental
7-HCFPA	1.00	1.05
11-HCFPA	2.00	1.99
15-HCFPA	3.00	2.80

1. This ratio will increase because of increasing concentration of 7-HCFPA versus unreacted 3-HCFPA as well as the formation of longer oligomers, and thus the progress of the oligomerization can be monitored by examining this ratio.

Oligomer formation proceeds only in the presence of oxidized iron centers and $Pt(NH_3)_4^{2+}$. Samples of 3-HCFPA that were chemically oxidized by PbO_2/H^+ followed by addition of $Pt(NH_3)_4^{2+}$ displayed increased numbers of doubly bridged irons. Samples that were not oxidized or were reduced by dithionite prior to addition of $Pt(NH_3)_4^{2+}$ did not form oligomers. If the only oxidation step is addition of PbO_2/H^+ to 3-HCFPA and the PbO_2 is removed before addition of $Pt(NH_3)_4^{2+}$, there is no appearance of a cyclic voltammetric wave indicative of the formation of $(\mu\text{-CN})_3\text{Fe}$ regardless of reaction time. In the absence of $(\mu\text{-CN})_3\text{Fe}$, all oligomer products must have a linear primary structure (Figure 1b). Since the terminal irons are always at the reactive oxidation state, the polymer continues to grow until all the platinum(II) salt complex has been consumed. The presence of these terminal oxidized irons along with internal reduced irons is confirmed by comparing the ^{15}N NMR spectra of 7-HCFPA isolated from an oligomer reaction to the spectra of reduced and oxidized 3-HCFPA (Table 2).

Once an Fe^{III} center has reacted with $Pt(NH_3)_4^{2+}$, it is reduced to Fe^{II}, and thus, all of the iron sites internal to the polymer are unable to react further. However, internal iron centers can be reoxidized using an external oxidant and in the presence of excess $Pt(NH_3)_4^{2+}$ form $(\mu\text{-CN})_3\text{Fe}$ sites resulting in a 2-dimensional oligomer (Figure 1c). For example, if the PbO_2 is not removed from the reaction mixture prior to the introduction of $Pt(NH_3)_4^{2+}$, then a two-dimensional structure is formed, as evidenced by the growth of a $(\mu\text{-CN})_3\text{Fe}$ cyclic voltammetric wave with $E_{1/2} = 1.1$ V vs SCE. If the oxidizing agent is strong enough, $(\mu\text{-CN})_3\text{Fe}$ can also be oxidized and allowed to react to form a 3-dimensional network. Branching can also be achieved via electrochemical oxidation. Since the redox potential of the iron center shifts positively by several hundred millivolts per cyanide bridge, it is possible to selectively oxidize $(\mu\text{-CN})_1\text{Fe}$ without oxidizing $(\mu\text{-CN})_2\text{Fe}$. For example, holding the working electrode at 0.60 V vs SCE in a solution initially containing only 3-HCFPA and $Pt(NH_3)_4^{2+}$ results in the creation of linear oligomers, indicated by the growth of the $(\mu\text{-CN})_2\text{Fe}$ cyclic voltammetric wave and no wave for $(\mu\text{-CN})_3\text{Fe}$. Increasing the working electrode potential to 0.8 V results in creation of oligomers with 2-dimensional structure as evidenced by growth of the $(\mu\text{-CN})_3\text{Fe}$ cyclic voltammetric wave. At a slightly more positive potential, it is possible to oxidize $(\mu\text{-CN})_3\text{Fe}$ and form a 3-dimensional polymer network. However, this 3-dimensional network is insoluble and forms a film on the surface of the working electrode. Thus, careful choice of the reaction potential allows one to select the predominant iron coordination environment and therefore the structure of the product polymers. Therefore in the poly-HCFPA system, voltammetric control during polymer electrosynthesis allows one to selectively generate polymers having specific morphologies. This redox-switched growth mechanism provides for an unusual (and simple) degree of synthetic control over the final polymer structure.

Table 2. ^{15}N NMR Peak Positions and Assignments

sample	δ (ppm)[a]	assignment
reduced 3-HCFPA	−95	equatorial cyanide
	−100	axial cyanide
	−270 t	bridging cyanide split by Pt
	−395 it	ammine
oxidized 3-HCFPA	820	equatorial cyanide
	70	axial cyanide
	−75 d	bridging cyanide
	−415 i	ammine
$[\text{7-HCFPA}]^{2-}$ isomer mixture	720	equatorial cyanide on Fe^{III}
	−70	bridging cyanide on Fe^{III}
	−95	equatorial cyanide on Fe^{II}
	−270 m	bridging cyanide on Fe^{II}
	−400 i	ammine

[a] Key: d, doublet; t, triplet; m, multiplet; i, inverted peak.

NMR Characterization of Oligomers. There are three structural isomers possible for 7-HCFPA depending on whether the 3-HCFPA units react via axial or equatorial cyanide ligands (Figure 5). An oligomer mixture synthesized by reacting oxidized 3-HCFPA with $Pt(NH_3)_4^{2+}$ was run through a 2.3 m column of Sephadex G-25. Seven fractions were collected, and cyclic voltammetric analysis indicated that two of these fractions corresponded to pure 7-HCFPA; two others were identified as 11-HCFPA and 15-HCFPA. The remaining fractions were mixtures of longer chain oligomers. ^{13}C and ^{15}N NMR methods were used to further characterize 3-HCFPA, the two fractions of 7-HCFPA, 11-HCFPA, and 15-HCFPA. Both the ^{13}C and ^{15}N NMR spectra of the cyanides are sensitive to the coordination environment of the iron and can be identified as a bridging, terminal-equatorial, or terminal-axial cyanide; however, ^{13}C NMR was found to be the best for quantitative analysis.

The ^{13}C NMR spectrum of 3-HCFPA has three peaks at δ 177.0, 171.9, and 168.4 ppm. The signal of the carbon in the bridging cyanide is expected to be shifted most downfield because formation of the CN−Pt bond reduces the electron density about this carbon. Thus, the peak at δ 177.0 ppm is assigned to the bridging cyanide carbon. This is further supported by sidebands indicating coupling with the ^{195}Pt spin $^1/_2$ nuclei. The lower electron density on the bridging cyanide will increase the π-back-bonding interactions associated with the trans (axial) cyanide carbon, thereby shifting its resonance upfield. The cyanides which are cis to the bridging cyanides and referred to here as the equatorial cyanides will most closely

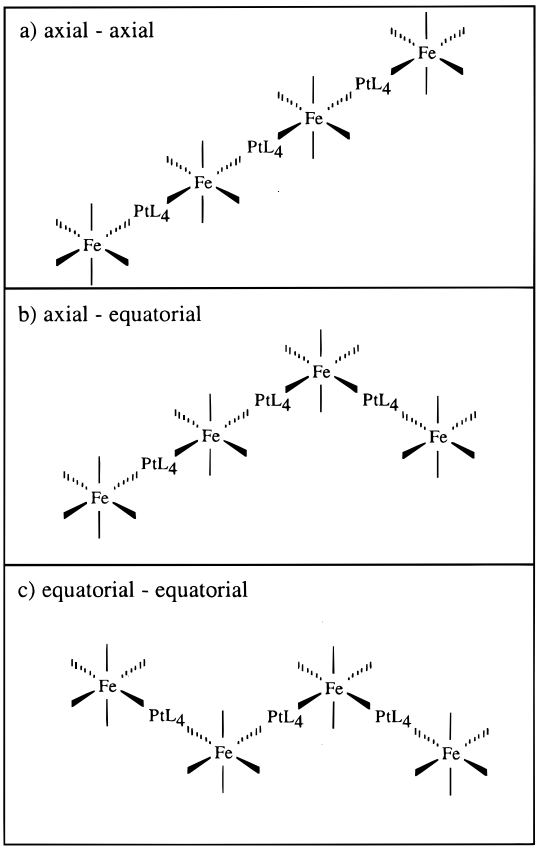

Figure 5. Structural isomers of 7-HCFPA; (a) axial−axial; (b) axial−equatorial; (c) equatorial−equatorial.

Table 3. ^{13}C NMR Peak Positions and Experimental (Theoretical) Peak Integrations

sample	bridging δ (ppm) peak integrations	equatorial δ (ppm) peak integrations	axial δ (ppm) peak integrations
3-HCFPA	177.0	171.9	168.4
	2.16 (2.00)	8.00 (8.00)	1.84 (2.00)
7-HCFPA	173.1	169.2	166.0
a−e, a−a	4.10 (4.00)	6.25 (6.20)	1.65 (1.80)
7-HCFPA	181.2	172.6	169.1
e−e	4.26 (4.00)	4.00 (4.00)	3.74 (4.00)
11-HCFPA[a]	175.2	171.4	168.2
	8.25 (8.00)	12.3 (9.60)	3.50 (6.40)
15-HCPFA[a]	173.1	169.4	165.6
	12.7 (12.0)	17.1 (14.4)	6.2 (9.60)

[a] Oligomer samples were mixtures of all structural isomers, and peak positions were tabulated on the basis of the strongest signal within the multiplet.

resemble the cyanides of free ferrocyanide, which has a ^{13}C peak at δ 171.0 ppm. On the basis of these arguments, the peak at δ 168.4 ppm is assigned to the axial cyanide carbon and the peak at δ 171.9 ppm to the equatorial cyanides. Integration of the peaks yields a ratio of 2.16 bridging to 8.00 equatorial to 1.84 axial, which is within the experimental error of the expected ratio of 2.00/8.00/2.00 for 3-HCFPA (Table 3).

This analysis was applied to the oligomer fractions. To differentiate the cyanide carbons on the terminal irons from the internal ones, the terminal irons were maintained in the oxidized state. The heavy shielding effect of the paramagnetic iron shifted the signals of the terminal cyanide carbons far upfield close to the peak position of ferricyanide at ~3600 ppm, while the signals of the interior iron cyanide carbons appeared near 170 ppm. The ^{13}C NMR spectra of the various fractions are summarized in Table 3. Comparison of the integrated peak

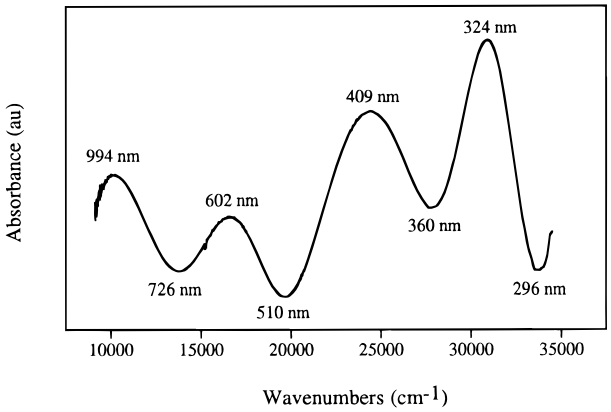

Figure 6. UV−vis interferometry of poly-HCFPA as a film on ITO showing interference fringes.

Table 4. Distribution of Bridging, Equatorial, and Axial Cyanides for Different Structural Isomers of 7-HCFPA

structural isomer	bridging	equatorial	axial
axial−axial	2 near Fe^{III}	8	none
	2 away from Fe^{III}		
axial−equatorial	2 near Fe^{III}	6	1 trans to Fe^{III}
	2 away from Fe^{III}		1 cis to Fe^{III}
equatorial−equatorial	2 near Fe^{III}	4	2 trans to Fe^{III}
	2 away from Fe^{III}		2 cis to Fe^{III}

ratios with the expected theoretical ratios allowed identification of one of the 7-HCFPA fractions as a pure equatorial−equatorial isomer fraction and the other fraction as a mixture of axial−equatorial and axial−axial isomers as shown in Figure 5 (Tables 3 and 4). While the agreement between theoretical and experimental values is good for 3-HCFPA and the isomers of 7-HCFPA, the predicted percentages of equatorial cyanides for 11-HCFPA and 15-HCFPA are too low if one assumes all cyanides are equally reactive (Table 3). This may indicate that as the oligomer grows, steric interactions enhance the reactivity of equatorial cyanide sites, over axial sites perturbing the expected statistical reaction ratios.

UV−Vis Interferometry of Polymer Films. Thin films of polymer formed by electrochemical oxidation of the polymer on an ITO surface yielded an optical interference pattern in the visible region (Figure 6). The intensity of the interference bands precluded observations of electronic transitions, however, this pattern was found to offer an excellent method for determining the thickness of the polymer films.

Consider a Fabry−Perot etalon illuminated from one side with a white light source, the expected transmission spectrum is predicted by the Airy formula[8]

$$\frac{I_{\text{trans}}}{I_{\text{max}}} = \left[1 + F \sin^2\left(\frac{2\pi n_{\text{D}} t}{\lambda}\right)\right]^{-1} \quad (1)$$

where I_{trans} is the transmitted intensity, I_{max} is the incident intensity, F is finesse of the etalon, n_{D} is index of refraction of the material in the etalon, t is thickness of the etalon, and λ is the wavelength of light. From this, chromatic fringes are expected to be separated as[9]

$$n_{\text{D}} t = \frac{n}{2}\left(\frac{1}{\lambda_1} - \frac{1}{\lambda_2}\right)^{-1} \quad (2)$$

(8) Tolansky, S. *Multiple-beam Interferometry of Surfaces and Films*; Clarendon Press: Oxford, U.K., 1948.
(9) Conley, R. T. *Infrared Spectroscopy*; Allyn & Bacon, Inc.: Boston, MA, 1966.

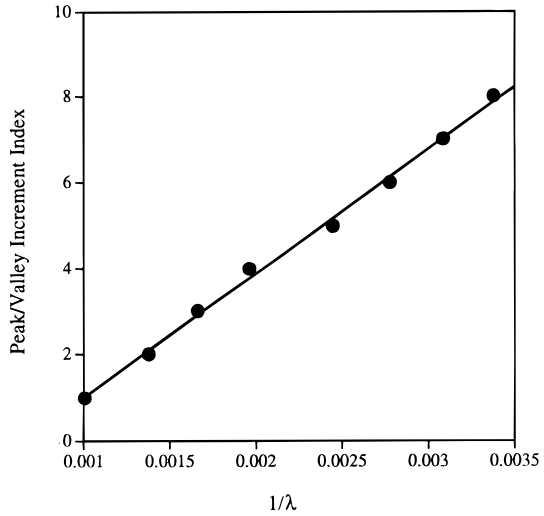

Figure 7. Optical thickness of a polymer film can be determined by fitting the inverse wavelength of the peaks and valleys of the UV−Vis interferogram. Line of best fit is $y = 2890x - 1.89$, with an r^2 of 0.997. This implies that the film has an actual thickness of 2890/4 nm, or 723 nm.

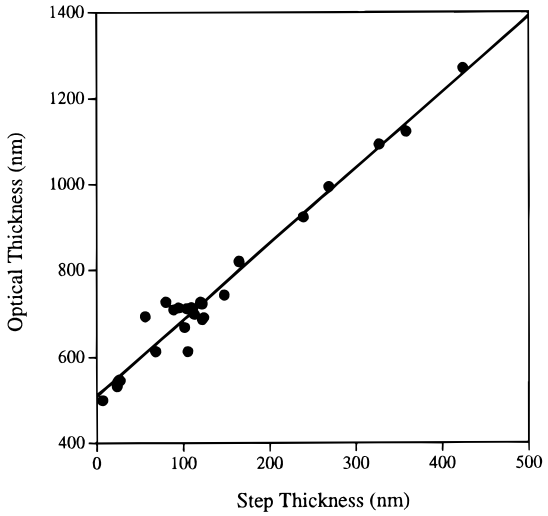

Figure 8. Optical thickness as calculated from interferograms correlated with the step thickness measured by profilometer. The fit suggests an index of refraction of 1.8 for the polymer film, and the *y*-intercept of 510 is the optical thickness of the ITO.

where $n_D t$ is the optical thickness of the film, λ_1 and λ_2 are two arbitrarily selected interference peaks, and n is the number of fringes between the two selected peaks. A more accurate value for the film thickness can be obtained if the inverse wavelengths of the peaks and valleys in the interferogram are plotted versus an increment scale. The slope of the line of best fit is 4 times the optical thickness of the etalon (Figure 7).

A profilometer was used to measure the actual film thickness, which was correlated with the optical thickness (Figure 8). The slope indicates that the film has an approximate index of refraction of 1.8 (slope of the line). A nonzero *y*-intercept is obtained due to the ITO coating, which has an estimated thickness of 300 nm and approximate index of refraction of 2.

The thickness of the polymer film can be controlled by adjusting either polymerization time or potential. Increasing polymerization time will lead to thicker films (Figures 9 and 10); however, the rate of film growth declines as the polymerization proceeds perhaps due to greater difficulty in charge transport from the electrode surface to the solution, where

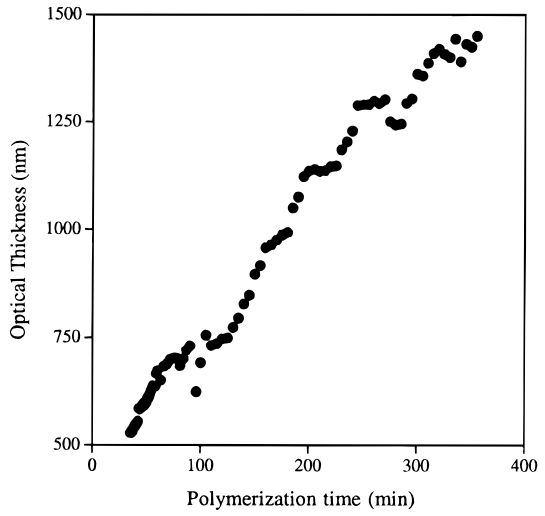

Figure 9. Increase in polymer film optical thickness with polymerization time as monitored in situ with the working electrode held at 1.0 V vs SCE.

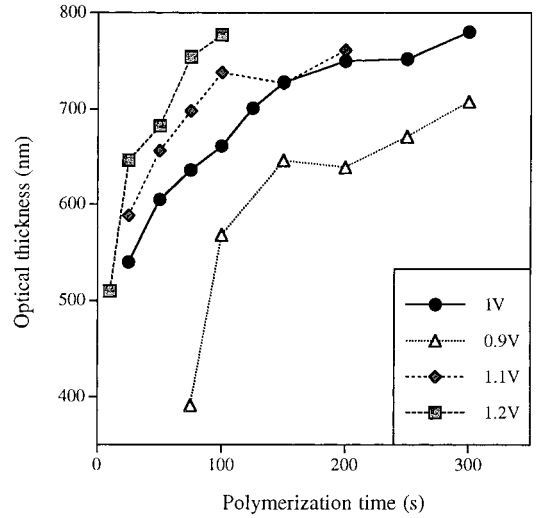

Figure 10. Increase in optical thickness with higher polymerization time or potential.

polymerization takes place. This suggests there is a maximum film thickness achievable at any particular polymerization potential, regardless of polymerization time. As the polymerization potential is increased, the rate of film growth as well as the maximum possible film thickness also increases. However, as noted previously, potential control also affects polymer structure.

Polymer Branching. The dependence of the $[Fe^{III/II}(CN)_6]^{3-/4-}$ redox potential on the number of bridging cyanides around a particular Fe center can also be used to characterize poly-HCFPA. Each wave in the cyclic voltammograms of the polymer film (Figure 3c) can be integrated to determine the relative amounts of differently bridged electroactive iron centers, and from this, one can infer the degree of branching (DOB). The DOB is defined as the weighted average of the number of bridging cyanides on each electroactive iron. As polymerization continues at a given potential, the degree of bridging will increase the DOB (Figure 11). This increase is due to the changes in relative populations of $(\mu\text{-CN})_i\text{Fe}$. For short polymerization times, the predominant species is $(\mu\text{-CN})_1\text{Fe}$ (Figure 12). As polymerization continues, $[(\mu\text{-CN})_1\text{Fe}]$ declines and $[(\mu\text{-CN})_2\text{Fe}]$ increases. Later, $[(\mu\text{-CN})_2\text{Fe}]$ peaks and is slowly replaced by $[(\mu\text{-CN})_3\text{Fe}]$. This pattern of increasing

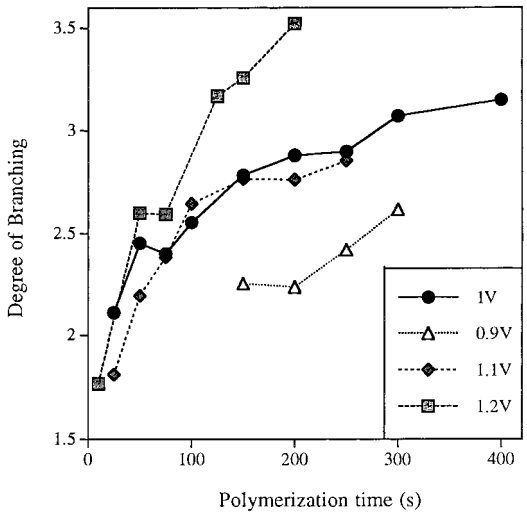

Figure 11. Increase on the degree of branching of polymer as a function of polymerization time and potential.

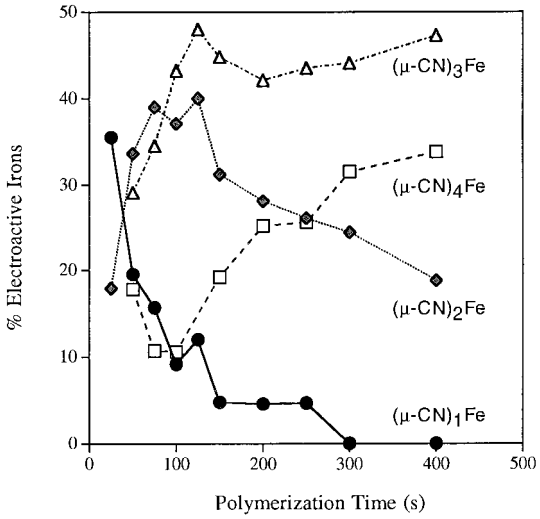

Figure 12. Distribution of electroactive species for increasing polymerization time showing a decrease in relative amounts of singly bridged irons and a corresponding increase in more highly bridged species.

polymer branching shows a slow conversion to more highly branched species, as opposed to for example a sudden conversion of $(\mu\text{-CN})_2\text{Fe}$ to $(\mu\text{-CN})_4\text{Fe}$. Thus, some idea of polymer morphology can be deduced from the value of the DOB. For instance, if the DOB is close to 2, then the primary structure of the polymer is predominantly linear. Note that the DOB provides no information about the secondary or tertiary structure. However, given the oligomer NMR results, polymer extension is more likely to occur at a bridging cyanide, which implies that the secondary structure includes many turns. As the DOB increases, there is more cross-linking within the polymer.

Degree of polymer bridging and polymer thickness are both dependent on synthetic conditions of polymerization. Thus, it is possible to vary polymerization potential and time independently to generate films of specific morphology and thickness, for example, to synthesize a series of films all with the same thickness but varying degrees of branching.

Conclusions

Oligomers of $[Fe^{II}(CN)_6{-}Pt^{IV}(NH_3)_4]$ units have been synthesized and separated by size exclusion chromatography. The dependence of the oligomer growth on the oxidation state of the $[Fe(CN)_6]^{3-/4-}$ within the oligomer is referred to as a redox-switched growth mechanism. Substantial control over the oxidation state can be achieved either chemically or electrochemically. The yield of a particular oligomer chain length can be maximized by changing the reactant ratios. However, for higher molecular weight oligomers, steric constraints appear to introduce reactivity differences between cyanide sites which distort the statistical population of isomers. Oligomers can be characterized by cyclic voltammetry to determine chain lengths, and specific structural isomers can be identified by NMR.

The inorganic coordination polymer thickness and morphology as characterized by visible light interferometry and cyclic voltammetry are found to be dependent both on polymerization time and on potential. The extent of polymer cross-linking can be expressed as the DOB which can be electrochemically controlled during polymerization. While no secondary or tertiary structural information can be obtained from the value of the DOB, it may be possible to model polymer growth to a first approximation as a random walk in three dimensions with the final tertiary structure being a random coil or, because of the presence of other growing chains, resembling a plate of spaghetti. It may also be possible to create a highly ordered structure if there are appropriate driving forces. One example of an ordered structure would be a series of parallel filaments if the DOB is close to 2, or the formation of sheet structures cross-linked between adjacent sheets at a higher DOB. It is likely the actual polymer morphology is between these two extremes with areas of homogeneity surrounded by random structures.

Acknowledgment. Support by the National Science Foundation under Grant No. CHE-9631380 is acknowledged.

IC980390E